Journal of Solid State Chemistry **152,** 421–427 (2000)
doi:10.1006/jssc.2000.8699, available online at http://www.idealibrary.com on IDEAL®

Paracrystal Formation from $Ni_{1-x}O$ and CaO upon Interdiffusion

Mei-Li Jeng and Pouyan Shen[1]

Institute of Materials Science and Engineering, National Sun Yat-sen University, Kaohsiung, Taiwan

Received November 29, 1999; in revised form February 28, 2000; accepted March 3, 2000

$Ni_{1-x}O$ and CaO powders 1:4 in molar ratio were sintered and annealed at 1200°C for 300 h or 1400°C for 1–80 h to investigate interdiffusion-induced defect clusters in the two rock salt-type oxides by analytical electron microscopy. Paracrystalline array of defect clusters ca. 3.2 and 1.6 times the lattice spacing of the average structure formed, respectively, from 8 mol% Ca dissolved $Ni_{1-x}O$ particles and 10 mol% Ni dissolved CaO matrix grains. The formation of paracrystal in the two oxides can be explained by the substitution of isovalent but size-mismatched dopant for cation in octahedral sites and resultant Ni^{3+} in tetrahedral interstitial sites to generate a considerable number of volume- and charge-compensating defects. The undersized dopant, i.e., nickel cation in CaO, may also directly reside in interstitial tetrahedral site; hence there is a higher concentration of defect clusters than the case of Ca^{2+}-doped $Ni_{1-x}O$. The paracrystal formed predominantly at the $Ni_{1-x}O$/CaO interface due to interdiffusion kinetics and a beneficial lower strain and interfacial energy.

Key Words: **paracrystal; $Ni_{1-x}O$; CaO; interdiffusion; dopant.**

1. INTRODUCTION

In this work, the $Ni_{1-x}O$/CaO composites prepared by sintering and then annealing in air were studied by analytical electron microscopy (AEM). We focused on the effect of isovalent but size-misfit dopant and resultant Ni^{3+} in tetrahedral interstitial sites on defect clustering of rock salt-type oxides.

Aliovalent dopant cations are known to cause defect clustering and phase changes of ionic crystals at high temperatures. The 3d transition metal monoxides with the rock salt structure have been extensively studied in this regard (1–20). $Fe_{1-x}O$, having a considerable degree of nonstoichiometry ($x \leq 0.15$ (2)), was known to possess defect clusters of 4:1 type with 4 octahedral vacant sites surrounding one Fe^{3+}-filled tetrahedral interstitial site (3). When aged at high temperatures, the 4:1 clusters may assemble into larger units (e.g., 13:4, 16:5 and form a paracrystal (4, 5)) which order further into Fe_3O_4 spinel or other ordered phases: p″ and p‴ (6, 7). (The paracrystalline distribution is such that the spacing between defect clusters tends to be maintained fairly constant but relative lateral translations may occur more variably; hence, there is negligible diffraction intensity beyond first order (4, 5).)

In contrast to $Fe_{1-x}O$, $Ni_{1-x}O$ has a very small x (ca. 0.001 at 1500°C (8)) and the occurrence of defect clustering is uncertain, whether from the theoretical point of view (9, 10) or based on experimental results (11–15). There is, however, clearer experimental evidence of defect clustering in cation-doped $Ni_{1-x}O$. For example, Zr-doped or (Zr, Y) codoped $Ni_{1-x}O$ was found by AEM to transform to a paracrystal and then Ni_3O_4 spinel when annealed at 1300°C or 1600°C (16, 17). In the case of $Co_{1-x}O$ with a moderate x (ca. 0.01 (18)), spontaneous oxidation to form Co_3O_4 spinel was known to occur by cooling below 900°C (19). Paracrystal and the spinel phase, however, form above 900°C for (Zr, Y)-codoped $Co_{1-x}O$ (20).

Here we choose the $Ni_{1-x}O$–CaO system having a considerable mutual solid-solubility (21) to study the effect of isovalent, but size-mismatched, dopant cations and resultant Ni^{3+} in tetrahedral interstitial sites on defect clustering of the rock salt-type oxides. Since the Ca^{2+} ion is much larger in size than Ni^{2+} ion in coordination number (C.N.) 6 of the oxygen environment (22), a considerable amount of volume-compensating defects due to substitution of Ca^{2+} for Ni^{2+} and vice versa is expected. It is of interest to find out whether or not the Ca-doped $Ni_{1-x}O$ or Ni-doped CaO exhibits paracrystal instead of dislocations as a compensation of volume misfit of the cations. Our previous defect chemistry consideration of Zr-doped $Ni_{1-x}O$ or (Zr,Y)-codoped $Ni_{1-x}O$ indicated that both charge and volume compensating defects are involved in the generation of 4:1 and larger defect cluster units (17). As to the present case of Ca-doped $Ni_{1-x}O$ or Ni-doped CaO, the dopant ions are predominantly isovalent with respect to the host cation. Still it is possible that volume-compensating effect of Ca^{2+} and Ni^{2+} caused the formation of cation vacancies and charge compensating nickel interstitials. It is of interest to find out

[1] To whom correspondence should be addressed. Fax: +886-7-5254099. E-mail: pshen@mail.nsysu.edu.tw.

0022-4596/00 $35.00

if undersized dopant Ni^{2+} is more effective than oversized dopant Ca^{2+} in generating defect clusters in CaO and $Ni_{1-x}O$, respectively. Research in the NiO–CaO system is thus of fundamental importance to understanding the defect chemistry of rock salt-type oxide with isovalent but size-mismatched cation dopant.

2. EXPERIMENTAL

Reagent grade $Ni_{1-x}O$ (Cerac, 99.99%, 100 mesh) and CaO (Cerac, 99.99%, 325 mesh) powders were used to prepare powder mixture batches of $Ni_{1-x}O$/CaO (1:4 molar ratio). The powder batches were ball-milled in deionized water, oven dried at 100°C, and dry pressed at 650 MPa to form pellets ca. 5 mm in diameter and 2 mm in thickness. The $Ni_{1-x}O$/CaO pellets were fired at 1200°C for 300 h and 1400°C for 1, 5, 10, 20, and 80 h in an open-air furnace and cooled in the furnace with a cooling rate of 5°C/min or quenched in air.

X-ray diffraction (XRD, Cu$K\alpha$, 40 kV, 20 mA at 0.05° and 3 s per step up to 2θ angle 105°) was used to identify the phases. The calculated lattice parameters from each d-spacing were plotted against $\cos^2\theta/\sin\theta$ and extrapolated to $\theta = 90°$ to obtain the precise lattice parameter a_o (23). Scanning electron microscopy (SEM, JSM6400 at 20 kV) was used to study the distribution of $Ni_{1-x}O$ particles in the sintered CaO matrix. Thin sections of the samples were Ar-ion milled to electron transparency. AEM (JEOL 3010 instrument operating at 300 kV) was used for imaging and point-count energy dispersive X-ray (EDX) analysis. The EDX analysis was performed using K shell counts for Ni and Ca and the principle of ratio method without absorption correction (24). The error of composition measurement was estimated to be within $\pm 5\%$.

3. RESULTS

3.1. SEM and XRD

SEM indicated that all the fired composites contain inter- and intragranular $Ni_{1-x}O$ particles in a matrix of CaO grains as represented by the sample fired at 1400°C for 10 h (Fig. 1). XRD indicated further that all the composites contain two rock salt-type oxides with lattice parameters of 0.420 and 0.480 nm, for Ca-dissolved $Ni_{1-x}O$ and Ni-dissolved CaO, respectively, indicating that solid solubility between CaO and $Ni_{1-x}O$ has been reached for all samples. The Ca-dissolved $Ni_{1-x}O$ has a larger lattice parameter than pure $Ni_{1-x}O$ (0.4177 nm, JCPDS file 4-0835) and Ni-dissolved CaO has a smaller lattice parameter than pure CaO (0.4811 nm, JCPDS file 4-0777). The defect clustering of CaO and $Ni_{1-x}O$ due to mutual solid solution was further revealed by AEM in the following.

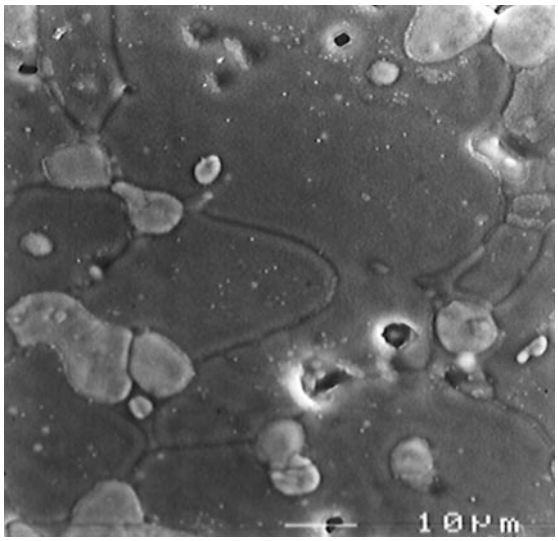

FIG. 1. SEM (secondary electron image) of $Ni_{1-x}O$/CaO (1:4 in molar ratio) composite fired at 1400°C for 10 h showing inter- and intragranular $Ni_{1-x}O$ particles in the matrix of CaO grains.

3.2. AEM

Electron diffraction indicated that the relatively small (submicrometer-sized) $Ni_{1-x}O$ particles have rotated into a parallel epitaxial relationship with respect to the host CaO grain for all the samples (25). In this connection, thermally activated Brownian rotation of intragranular particles toward epitaxial orientations has been reported to occur above a critical temperature for anchorage release, i.e., debonding of atoms, at the interface for a number of oxide composite systems: $Ni_{1-x}O$/Y-PSZ (26), $Ni_{1-x}O/NiAl_2O_4$ (27), and $Co_{1-x}O$/Y-PSZ (28). The well-developed (111) CaO/$Ni_{1-x}O$ interface of the parallel epitaxial $Ni_{1-x}O$ particle is free of misfit dislocation (25).

A second phase that caused side-band diffraction spots was developed from both the $Ni_{1-x}O$ particles (Fig. 2) and the CaO host grain (Fig. 3) close to the $Ni_{1-x}O$/CaO interface for all samples as represented by the composite fired at 1400°C for 20 and 80 h, respectively. Selected area electron diffraction patterns in Figs. 2a and 3a indicated that the spacing of such satellite diffraction spots are ca. 1/6.4 and 1/3.2 times that of the fundamental spots (e.g., the spot next to 200) of the two rock salt-type oxides, respectively. Dark field images (Figs. 2b and 3b) indicated that the side-band spots, with negligible diffraction intensity beyond first order, were diffracted from inhomogeneous domains, in accordance with paracrystalline distribution of defect clusters. (Analogously, Monte Carlo Simulation has proved that paracrystalline array of defect clusters (e.g. 13:4 and 16:5 derived from 4:1) inhomogeneously embedded in the rock-salt structure gave side-band X-ray diffraction spots for $Fe_{1-x}O$ single crystal (4, 5).) It should be noted that

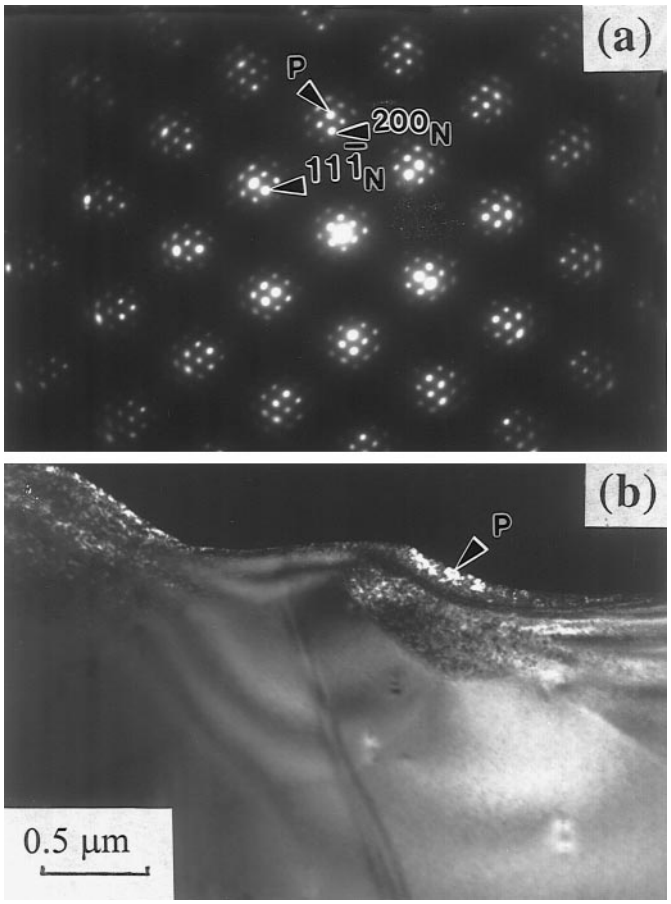

FIG. 2. (a) Selected area electron diffraction pattern in [011] zone axis showing fundamental and satellite spots of Ca-doped intergranular $Ni_{1-x}O$ particle. (b) Transmission electron microscopic (TEM) image (dark field image) taken with satellite spot (arrowhead), $Ni_{1-x}O$/CaO composite fired at 1400°C for 20 h.

nonepitaxial intergranular particles showed more clearly the side-band diffraction spots of paracrystal than epitaxial intragranular particles, because the latter case showed double diffraction spots from the epitaxial phases which are hard to tell from side-band diffraction spots.

Point-count EDX analysis also indicated that the paracrystal-containing area close to the $Ni_{1-x}O$/CaO interface has a higher dopant level than the rest area of the $Ni_{1-x}O$ and CaO phases. In the case of Ca-doped $Ni_{1-x}O$ particle, the Ca content is ca. 8 and 6 mol% for the paracrystal and the rest area, respectively. As for the Ni-doped CaO host, the Ni content is ca. 10 and 4 mol% for the paracrystal and the rest area, respectively. Inward diffusion of Ca and outward diffusion of Ni for the $Ni_{1-x}O$ particle was manifested by point count EDX concentration profiles across the $Ni_{1-x}O$/CaO interface for an intragranular $Ni_{1-x}O$ particle in the composite fired at 1400°C for 80 h (Fig. 4).

The samples quenched in air showed paracrystalline distribution of defects basically the same as that found in samples cooled in the furnace, indicating that the paracrystal formation was formed upon annealing at high temperatures. Our previous study of (Zr,Y)-codoped $Ni_{1-x}O$ (16, 17) also indicated that it is annealing at high temperature rather than cooling that caused interdiffusion and hence considerable dopant level for the formation of paracrystals and then Ni_3O_4-type spinel. The fact that paracrystals formed close to the interface of the diffusion couples with a relatively high dopant level is in accordance with this interpretation.

The paracrystal hardly developed into spinel superstructure for the present samples. The composite fired at 1200°C for 300 h showed also paracrystal for both the Ca-doped $Ni_{1-x}O$ and Ni-doped CaO (not shown) and the mutual solid solubility is not much different from that at 1400°C.

4. DISCUSSION

4.1. Defect Chemistry of Cation-Doped $Ni_{1-x}O$ and CaO

(a) Effect of Ni^{3+} in $Ni_{1-x}O$. Generation of an electron hole in the $Ni_{1-x}O$ lattice may proceed through the follow-

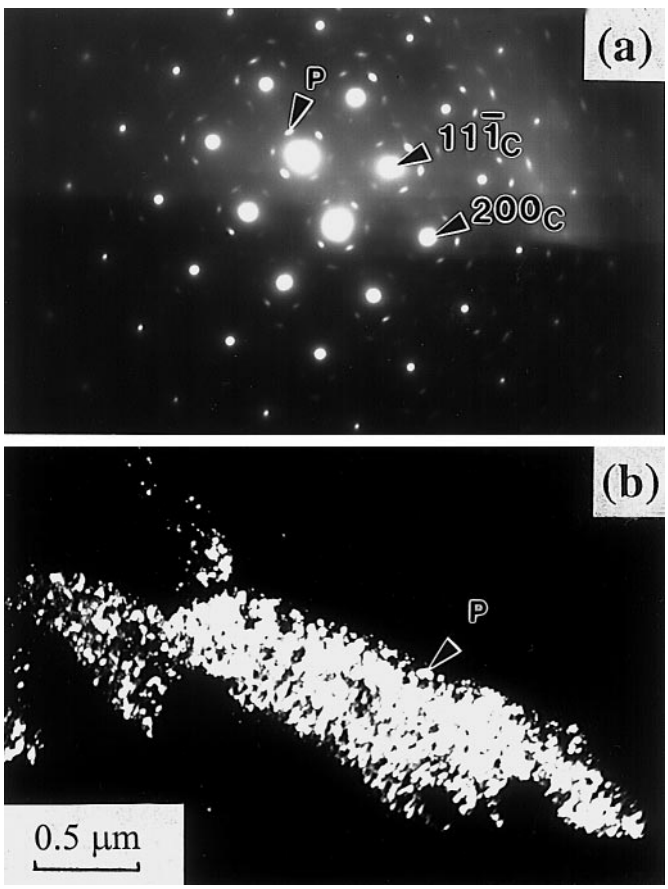

FIG. 3. (a) Selected area electron diffraction pattern in [110] zone axis showing fundamental and satellite spots of Ni-doped CaO matrix grain. (b) TEM image (dark field image) taken with satellite spot (arrowhead), $Ni_{1-x}O$/CaO composite fired at 1400°C for 80 h.

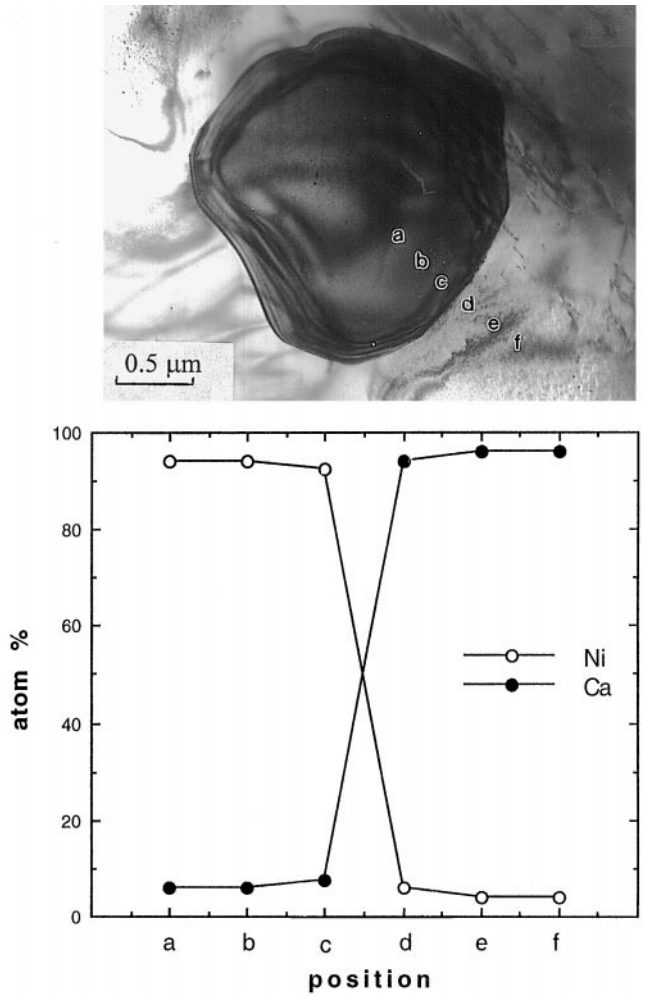

FIG. 4. TEM (bright field image) and point-count EDX concentration profiles (a to f) across the $Ni_{1-x}O$/CaO interface for intragranular $Ni_{1-x}O$ particle, $Ni_{1-x}O$/CaO composite fired at 1400°C for 80 h.

ing equations (29, 30) in Kröger–Vink notation (31):

$$\tfrac{1}{2}O_2 \text{--} V_{Ni}^{x} + O_O^{x} \qquad [1]$$

$$V_{Ni}^{x} \text{--} V_{Ni}' + h^{\bullet} \qquad [2]$$

$$V_{Ni}' \text{--} V_{Ni}'' + h^{\bullet} \qquad [3]$$

In this notation, the type of imperfection is indicated by a major symbol, the location is described by a subscript, and finally the charge of the defect relative to the normal lattice is indicated by a superscript. Here, O_O^{x} signifies a neutral charged oxygen atom in the normal lattice site; V_{Ni}^{x}, V_{Ni}', and V_{Ni}'' represents a neutral, single, and double negatively charged nickel vacancy, respectively; and $h^{\bullet}$ signifies electron hole ($Ni_{Ni}^{3+\bullet}$ or simplified as $Ni_{Ni}^{\bullet}$). The singly charged nickel vacancy V_{Ni}' is in fact $[V_{Ni}'' + Ni_{Ni}^{\bullet}]$ (V_{Ni}'' associated with an electron hole localized to form a bound pair of point defects on the octahedral Ni sites) (30). In general, a higher temperature oxidation through Eqs. [1]–[3] is expected to increase the Ni^{3+}/Ni^{2+} ratio. A pronounced effect of temperature on the increase of Ni^{3+} concentration (>0.1%) is indeed indicated by the occurrence of a dark green color in the fired $Ni_{1-x}O$ (8). In addition to the temperature effect, theoretical calculation indicated that nickel vacancy concentration increases by a factor of about 40 over the bulk value for the (211)/[011] twist grain boundary of $Ni_{1-x}O$ at 1000 K (32). Nevertheless the Ni^{3+}/Ni^{2+} ratio of the $Ni_{1-x}O$ polycrystals was still not high enough to cause appreciable defect clustering or the formation of the superstructures as proved experimentally by annealing the $Ni_{1-x}O$ polycrystals at 1873 K for 300 h (17).

(b) Effect of Ca^{2+} in $Ni_{1-x}O$. The present XRD results indicate that the lattice parameters of CaO and $Ni_{1-x}O$ are compensating upon solid solution. In addition, Ca^{2+} ion is in six-fold coordination in the rock salt structured CaO. Thus it is conceivable that Ca^{2+} dopant resides in octahedral substitutional sites instead of interstitial tetrahedral sites of the $Ni_{1-x}O$ lattice. The Ca^{2+} dopant, being oversized, is expected to cause volume compensating defect clusters $[V_{Ni}'' + Ni_{Ni}^{\bullet}]$ through the following equation:

$$CaO \xrightarrow{NiO} Ca_{Ni}^{x} + [V_{Ni}'' + Ni_{Ni}^{\bullet}] + h^{\bullet} + O_O^{x}. \qquad [4]$$

Here Ca_{Ni}^{x} signifies a noncharged calcium at nickel sites in the crystal lattice. It is also possible that the volume compensating effect due to the substitution of Ca^{2+} (effective ionic radii, 0.1 nm) with Ni^{2+} (0.069 nm) in C.N. 6 (22) forced $Ni_{Ni}^{\bullet}$ to enter the interstitial tetrahedral site, i.e., $Ni_i^{\bullet\bullet\bullet}$, and hence more charge-compensating cation vacancies through the following equation:

$$Ca_{Ni}^{x} + [V_{Ni}'' + Ni_{Ni}^{\bullet}] \text{--} Ca_{Ni}^{x} + [Ni_i^{\bullet\bullet\bullet} + 4V_{Ni}'' + 4Ni_{Ni}^{\bullet}]. \qquad [5]$$

Thus the 4:1 type defect clusters and the paracrystalline ordered state could be activated through reaction [5]. In this regard, theoretical calculation indicated that interstitial tetrahedral dopant can stabilize the 4:1 clusters and clusters of 4:1 clusters for 3d transition metal monoxides, e.g., Fe^{3+}-doped $Ni_{1-x}O$ and Mn^{3+}-doped $Co_{1-x}O$ (33).

Oxygen vacancies may also be introduced around Ca_{Ni}^{x} for volume and charge compensation, and hence affect the defect structure of the surrounding $Ni_{1-x}O$ lattice. In this connection, it is interesting to note the recent X-ray absorption study of zirconia using synchrotron radiation with regard to the change of oxygen coordination due to dopant (34). Their results indicated that oversized dopant Y^{3+} is 8-fold coordinated with nearby Zr^{4+} in 7-fold coordination

(i.e. an oxygen vacancy prefers to be associated with Zr^{4+}). On the other hand, an undersized dopant such as Fe was forced to compete with Zr ions for the oxygen vacancies in zirconia resulting in six-fold oxygen coordination for the dopant and a large disturbance to the surrounding next nearest neighbor (35). It remains to be studied whether or not the oversized Ca^{2+} in substitution for Ni^{2+} in rock salt-type oxide causes nearby Ni^{2+} in lower coordination analogous to the effect of oversized dopant Y^{3+} in zirconia (34).

(c) Effect of Ni^{2+} in CaO. As to Ni^{2+} dissolving in the CaO lattice, it should substitute for Ca^{2+} in C.N. of 6 in order to compensate the cell volume of the solid solution as mentioned. The undersized dopant Ni^{2+} in the Ca^{2+} site could also force further Ni^{2+} dopant to enter the interstitial site as $Ni_i^{\cdots}$, which then induced charge-compensating cation vacancies and 4:1 defect clusters through the following equation:

$$NiO \xrightarrow{CaO} Ni_{Ca}^{x} + [Ni_i^{\cdots} + 4V_{Ca}'' + 5h^{\cdot}] + O_O^{x} \qquad [6]$$

where $h^{\cdot}$ could be associated with V_{Ca}'' to form V_{Ca}' or associated with Ni_{Ca}^{x} to form $Ni_{Ca}^{\cdot}$.

It is noteworthy that there is no paracrystal formed from CaO in $CaO/CaZrO_3$ composite fired at 1600°C for up to 320 h in air (25). This can be rationalized by negligible solid solubility of Zr^{4+} in CaO lattice under such a firing condition.

(d) Spacing between defect clusters. The spacing between defect clusters, i.e., the concentration of defect clusters, is affected by dopant level. For example, our previous study indicated that the dissolution of ca. 2 mol% Zr^{4+} caused the paracrystalline distribution of defects nearly 3.5 times that seen in the lattice parameter of Zr^{4+}-doped $Ni_{1-x}O$ (17). By contrast, the dissolution of ca. 2 mol% Zr^{4+} with codopant $Y^{3+} < 0.3$ mol% led to paracrystal distribution of defects nearly 2.5 times that seen in the lattice parameter (17), i.e., a higher concentration of defect clusters.

The paracrystalline distribution of defect clusters is nearly 3.2 and 1.6 times that seen in the lattice spacing of the average structure for Ca-doped $Ni_{1-x}O$ and Ni-doped CaO, respectively (Figs. 5a and 5b) as indicated by the spacing of side-band diffraction spots (Figs. 2 and 3). (The exact nature of 4:1-type derived defect clusters in the two cases may be different as mentioned.) Thus the spacing between defect clusters in Ca^{2+}-doped $Ni_{1-x}O$ is ca. two times that of Ni^{2+}-doped CaO, in spite of a nearly equal solute content for the two cases. In other words, Ni^{2+} dopant in CaO is more effective than Ca^{2+} dopant in $Ni_{1-x}O$ to generate defect clusters, ca. 8 times difference in concentration. In this regard, $Ni_i^{\cdots}$, the ingredient of 4:1 and larger clusters as mentioned, may be more effectively

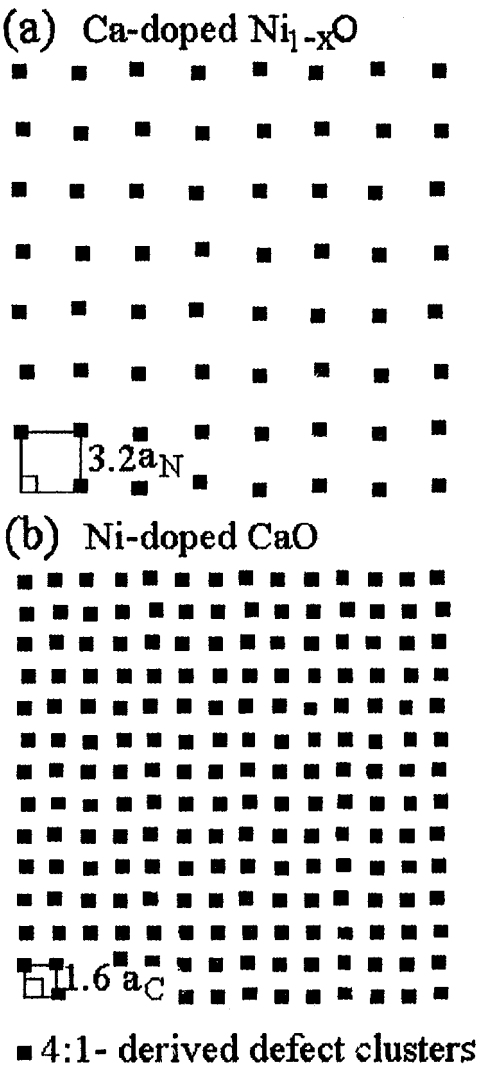

FIG. 5. Schematic drawing ([100] projection in real space) of paracrystalline distribution of 4:1-type-derived defect clusters (solid squares) with nearly 3.2 and 1.6 times that seen in the lattice spacing a_N (0.420 nm) and a_C (0.480 nm) of the average structure for (a) Ca-doped $Ni_{1-x}O$ and (b) Ni-doped CaO, respectively.

generated through Eq. [6] for Ni^{2+}-doped CaO than through Eqs. [4] and [5] for Ca^{2+}-doped $Ni_{1-x}O$.

(e) Spinel formation. The spinel phase hardly formed from the present $Ni_{1-x}O$ dissolved with ca. 8 mol% Ca, in sharp contrast to the spinel precipitation from $Ni_{1-x}O$ with a much less dopant level (2 mol%) of Zr or both Zr and Y (16, 17). Unlike Ca^{2+}, the Zr^{4+} and Y^{3+} dopants are aliovalent with respect to the Ni^{2+} being replaced and hence introduce more charge compensating defects for spinel phase to nucleate in the $Ni_{1-x}O$ lattice. Given a relatively high concentration of $Ni_i^{\cdots}$ in the case of $Ni_{1-x}O$ with the Zr^{4+} and Y^{3+} dopants (16, 17), there should be enough

4:1 clusters, i.e., $[Ni_i^{\bullet\bullet\bullet} + 4V''_{Ni} + 4Ni^{\bullet}_{Ni}]$, to form spinel phase with cations in both tetrahedral and octahedral sites. (A single 4:1 cluster has local topology similar to the spinel structure, but is not sufficiently large to constitute a spinel phase.)

It is noteworthy that furnace cooling of Al-doped $Ni_{1-x}O$ fired at 1600°C for 1–80 h caused exsolution of $NiAl_2O_4$ spinel at dislocation (36). In the present case of Ca-doped $Ni_{1-x}O$ or Ni-doped CaO, there is no equilibrium $CaNi_2O_4$-type spinel to be exsolved upon cooling. Under specified undercoolings, the coexisting $Ni_{1-x}O$ and CaO simply adjusted solute content across the interface without appreciable precipitation of Ni_3O_4-type spinel.

4.2. *Effect of Interdiffusion across Interface*

The present observations indicated that the CaO/$Ni_{1-x}O$ interface was the preferred nucleation site of the paracrystal. This could be due to a higher defect concentration near the interface. Alternatively, surface nucleation of the paracrystal is beneficial in minimizing strain and/or surface energies and can be facilitated by a higher diffusivity of cation vacancies at surface as proved for $Ni_{1-x}O$ (37).

The net number of vacancies near the interface must vary with time in the early stage of interdiffusion. This kinetic factor accounts for the Kirkendall pore formation at the $Co_{1-x}O$/yttria partially stabilized zirconia (Y-PSZ) interface for the $Co_{1-x}O$/Y-PSZ composite prepared via a sintering route (20). It should be noted that Kirkendall pore formation for ionic compound requires the motion of both cations and anions. There is a relatively larger flux of Co^{2+} (ca. 6 mol%) from $Co_{1-x}O$ into Y-PSZ compared to the reverse flux of Zr^{4+} (<2 mol%) and Y^{3+} (<1 mol%) at 1600°C (20). The flux of oxygen has also been proved by experiments. For example, microanalysis of an oxidized CoO–zirconia (CaO stabilized) eutectic (38) and parallel-detection electron energy-loss (PEEL) spectrometer analysis of $Co_{1-x}O$ coating on zirconia (CaO stabilized) (39) indicated a higher oxygen concentration for $Co_{1-x}O$ toward the interface, due to a relatively higher diffusivity of oxygen in zirconia than in $Co_{1-x}O$. This factor, along with unequal cation flux, accounts for the formation of Kirkendall pores at the $Co_{1-x}O$/Y-PSZ interface (20). By contrast, the mutual solid solubility of $Ni_{1-x}O$ and CaO are nearly equal and oxygen diffusivity is expected to be nearly the same for the two phases having the same rock salt-type structure. Thus, there is a net shortage of vacancies for the Kirkendall pore formation at the $Ni_{1-x}O$/CaO interface as interdiffusion proceeds with time. Without Kirkendall pores, the defect clusters could still reconcile the lattice mismatch ($\delta = (a_C - a_N)/a_N = 0.14$, where a_C and a_N are lattice parameters of Ni-doped CaO and Ca-doped $Ni_{1-x}O$, respectively). This is indicated by the devoid of misfit dislocations around the $Ni_{1-x}O$ particles having reached parallel epitaxial relationship with respect to the host CaO grains by a Brownian-type rotation process of particles in the bulk (25).

5. SUMMARY

1. Analytical electron microscopic observations revealed the formation of paracrystalline array of defect clusters from $Ni_{1-x}O$ particles and the CaO matrix grains due to mutual dissolution of isovalent dopant at 1200 and 1400°C.

2. The oversized dopant Ca^{2+} should reside in substitutional octahedral site of $Ni_{1-x}O$, whereas the undersized dopant Ni^{2+} both the substitutional octahedral and interstitial tetrahedral site of CaO in order to generate volume- and charge-compensating defects for further formation of paracrystal in the rock salt-type lattice.

3. Undersized dopant, i.e., Ni^{2+} in CaO, can also reside in interstitial tetrahedral site hence a larger number of defect clusters for Ni^{2+}-doped CaO than Ca^{2+}-doped $Ni_{1-x}O$, as indicated by paracrystalline array of defect clusters ca. 1.6 and 3.2 times that seen in the lattice spacing of the average structure, respectively.

4. The paracrystal formed predominantly at the $Ni_{1-x}O$/CaO interface due to interdiffusion kinetics and for a beneficial lower strain and interfacial energy at the interface.

REFERENCES

1. P. Kofstad, "Nonstoichiometry, Diffusion and Electrical Conductivity in Binary Metal Oxides," Wiley Interscience, New York, 1972.
2. B. E. F. Fender and F. D. Riley, "The Chemistry of Extended Defects in Non-Metallic Solids" (L. Eyring and M. O'Keefe, Eds.), North-Holland, Amsterdam, 1970.
3. C. R. A. Catlow and B. E. F. Fender, *J. Phys. C*: *Solid State Phys.* **8,** 3267 (1975).
4. T. R. Welberry and A. G. Christy, *J. Solid State Chem.* **117,** 398 (1995).
5. T. R. Welberry and A. G. Christy, *Phys. Chem. Minerals* **24,** 24 (1997).
6. P. Vallet and P. Raccah, *Mem. Sci. Rev. Metall.* **62,** 1 (1965).
7. B. Andersson and J. O. Sletnes, *Acta Crystallogr. A* **33,** 268 (1977).
8. H. G. Sockel and H. Schmalzried, *Ber. Bunsenges. Phys. Chem.* **72,** 745 (1968).
9. C. R. A. Catlow and A. M. Stoneham, *J. Am. Ceram. Soc.* **64,** 234 (1981).
10. R. W. Grime, A. B. Anderson, and A. H. Heuer, *J. Am. Ceram. Soc.* **69,** 619 (1986).
11. W. C. Tripp and N. M. Tallan, *J. Am. Ceram. Soc.* **53,** 531 (1970).
12. M. L. Volpe and J. Reddy, *J. Chem. Phys.* **53,** 1117 (1970).
13. C. M. Osburn and R. W. Vest, *J. Phys. Chem. Solids* **32,** 1331 (1971).
14. R. L. Lalauze and J. H. Meunier, *Oxid. Met.* **12,** 183 (1978).
15. J. Szuber, *J. Mater. Sci.* **19,** 1991 (1984).
16. P. Shen, S. Chen, and H. S. Liu, *Mater. Sci. Eng. A* **161,** 135 (1993).
17. J. Chen and P. Shen, *J. Solid State Chem.* **140,** 361 (1998).
18. S. M. Tomlinson, C. R. A. Catlow, and J. H. Harding, *J. Phys. Chem. Solids* **51,** 477 (1990).
19. M. Oku and Y. Sato, *Appl. Surf. Sci.* **55,** 37 (1992).
20. K. T. Lin and P. Shen, *J. Solid State Chem.* **145,** 739 (1999).
21. D. E. Smith, T. Y. Tien, and L. H. van Vlack, *J. Am. Ceram. Soc.* **52,** 460 (1969).
22. R. D. Shannon, *Acta Crystallogr. A* **32,** 751 (1976).
23. B. D. Cullity, "Elements of X-ray Diffraction," Addison-Wesley, Reading, MA, 1978.

24. D. B. Williams, "Practical Analytical Electron Microscopy in Materials Science," p. 157, Philips Electronic Instruments, Electron Optics Publishing Group, Mahwah, NJ, 1984.
25. M. L. Jeng, M.S. thesis, National Sun Yat-sen University, Taiwan, 1999.
26. J. Chen and P. Shen, *Scripta Metall.* **37,** 1287 (1997).
27. S. R. Wang and P. Shen, *Mater. Sci. Eng. A* **251,** 106 (1998).
28. K. T. Lin and P. Shen, *Mater. Sci. Eng. A* **270,** 125 (1999).
29. P. Kofstad, "Nonstoichiometry, Diffusion and Electrical Conductivity in Binary Metal Oxides," Wiley Interscience, New York, 1972.
30. A. Atkinson, A. E. Hughes, and A. Hammou, *Phil. Mag. A* **43,** 1071 (1981).
31. F. A. Kröger and H. J. Vink, *Solid State Phys.* **3,** 307 (1956).
32. D. M. Duffy, *Phil. Mag.* **50,** 143 (1984).
33. R. W. Grime, A. B. Anderson, and A. H. Heuer, *J. Phys. Chem. Solids* **48,** 45 (1987).
34. P. Li, I. W. Chen, and J. E. Penner-Hahn, *Phys. Rev. B* **48,** 10074 (1993).
35. P. Li, I. W. Chen, and J. E. Penner-Hahn, *J. Am. Ceram. Soc.* **77,** 118 (1994).
36. S. R. Wang and P. Shen, *J. Solid State Chem.* **140,** 38 (1998).
37. A. Atkinson and R. I. Taylor, *Philos. Mag. A* **43,** 979 (1981).
38. J. Bentley, S. McKernan, C. B. Carter, and A. Revoolevschi, "Electron Microscopy and Analysis," Inst. Phys. Conf. Ser. No. 138, Section 2, p. 39, JOP Bristol, UK, 1993.
39. H. I. Yoo and J. H. Lee, *J. Phys. Chem. Solids* **57,** 65 (1996).